Accepted Manuscript

Distributed fluorescent optical fiber proximity sensor: Towards a proof of concept

Ramona Gălătuș, Paul Faragó, Piotr Miluski, Juan Antonio Valles Brau

PII:	S1386-1425(18)30161-6
DOI:	doi:10.1016/j.saa.2018.02.044
Reference:	SAA 15848
To appear in:	*Spectrochimica Acta Part A: Molecular and Biomolecular Spectroscopy*
Received date:	30 November 2017
Revised date:	3 February 2018
Accepted date:	12 February 2018

Please cite this article as: Ramona Gălătuș, Paul Faragó, Piotr Miluski, Juan Antonio Valles Brau , Distributed fluorescent optical fiber proximity sensor: Towards a proof of concept. The address for the corresponding author was captured as affiliation for all authors. Please check if appropriate. Saa(2017), doi:10.1016/j.saa.2018.02.044

Distributed fluorescent optical fiber proximity sensor

Towards a proof of concept

Ramona Gălățuș[1], Paul Faragó[1], Piotr Miluski[2], Juan Antonio Valles Brau[3]

1. Technical University of Cluj-Napoca, str. Memorandumului nr. 28, Romania
2. Bialystok University of Technology, Wiejska 45D, 15-351 Bialystok, Poland
3. University of Zaragoza, Spain

Abstract: Fluorescent fibers are optical fibers which emit light as a response to an incident phenomenon, usually an incident light. Operation depends on the doping dyes, which determine specific fluorescence and optical characteristics useful in the development of optical sensors. In this work we propose a low-cost distributed proximity sensor implemented using a red fluorescent fiber, to provide a security option for a surface plasmon resonance system. Operation of the proposed sensor relies on having the incident illumination intensity varied by the presence or absence of an obstacle in the vicinity of the sensing element. This will influence the radiated fluorescence accordingly. The proposed setup for the implementation of the optical proximity sensor assumes having a high brightness LED deployed for axial fiber illumination and a blue LED for side illumination. Electronic processing then accounts for gain and digitization. Measurement results of the prototype validate the proposed concept.

Keywords: optical fibers, fluorescence, proximity distributed sensing.

* Ramona Gălățuș, E-mail: Ramona.Galatus@bel.utcluj.ro

1. Introduction

A fluorescent optical fiber is an optical fiber which emits light as a response to an incident phenomenon, e.g. fiber sensitive to molecular oxygen reported by a group of AT&T Bell Lab in 1989, high energy particles, UV or visible light, etc. [1, 2, 3]. The molecules of the organic dyes can be effectively excited due to their wide absorption band. The fluorescence intensity and lifetime in polymeric host strongly depend on the environmental conditions e.g. local molecular bindings, acidity, temperature and non-radiative excited state deactivation in the presence of quenchers. Numerous sensor have been developed based on fluorescence intensity modulation. Moreover, guiding properties of optical fiber can be used for transferred light modulation e.g. intensity and spectrum shape. This paper considers fluorescent fibers which emit light as a response to side illumination in the visible spectrum. One of the main benefits of fluorescent optical fibers is the increased flexibility of side illumination vs. traditional axial illumination [4]. Whereas axial illumination requires complicated and expensive coupling optics for confining the light radiation into the fiber core, side illumination is simply performed by illuminating the fiber cladding from an LED. Moreover, the advent of doping materials sensitive to light in the visible spectrum allowed for the employment of color LEDs in comparison to more expensive UV excitation sources as was the case in the past. These advantages motivate the employment of fluorescent optical fibers in the development of optical sensors.

Fluorescent fibers are a very attractive medium for the development of optical sensors. Indeed, sensitivity towards an incident phenomenon makes the fluorescent fiber readily a sensing element. One conclusive example is a position sensor proposed by M. F. Laguesse in [5], where side illumination is employed to induce fluorescence into the fiber, and the position of the illumination point is determined by measuring the illumination power at the two fiber ends. The author compares the proposed solution to an optical potentiometer. A similar approach was employed by J. D. Weiss in [6] for the implementation of a long-distance position sensor aimed for industrial applications. The optical potentiometer principle was also applied by Aiestaran et al. in [7] for the implementation of position sensors, after comparing different fiber colors to evaluate their applicability to position sensing.

Another application of fluorescent fibers is the nuclear particle detector proposed by A. D. Bross in [8]. In this application, scintillation radiation is produced within the fluorescent fiber as a result of exposure to nuclear particles. Other examples of fluorescent fiber optical sensors for particle detection account for molecular oxygen in [9], detection of UV radiation in [10], X-ray beam detection in [11], chloride ion detection in [12] or chemical species

detection in [13]. Each of these sensors employ the sensitivity of dye fluorescence on the particles of interest.

A similar principle enables the implementation of a variety of sensors for environmental monitoring. For exemplification, C. O. Egalon developed a relative humidity sensor in [4]. This solution employs a fluorescent fiber which produces fluorescence within the cladding material which is then transmitted along the fiber. The fluorescence magnitude in this solution is dependent on the surrounding humidity. Another application for environmental monitoring is a temperature sensor proposed by Wu et al. in [14]. This solution uses a fluorescent fiber and a pulse modulated signal source, followed by phase-locked detection. This solution is claimed to provide a very good resolution and precision for temperature monitoring.

Previous works reported by the authors employ the fluorescence spectral parameters for the implementation of UV [15, 16] and temperature [17] measurement systems. In each of these applications, the fluorescence wavelength or intensity are monitored in order to determine the parameters of the phenomenon which induced fluorescence.

Another approach for optical sensor development with fluorescent fibers is to have them deployed as illuminators [18]. For exemplification, previous work reported by the authors use fluorescent polymeric fibers for surface plasmon resonance (SPR) applications [19]. In such applications, the fluorescent fiber is used as a light source for the SPR sensor.

In this work, we propose a low-cost distributed proximity sensor intended to provide a security option for our SPR system previously reported in [20]. The proposed proximity sensor is developed around a 81 0087 red fluorescent fiber from Industrial Fiber Optics, which is applied to an Avago SFH250 photodiode to generate an equivalent voltage drop. Operation of the proposed sensor relies on having the incident illumination intensity varied by the presence or absence of an obstacle in the vicinity of the sensing element, which will influence the radiated fluorescence accordingly. This in turn will generate a variation of the photodiode voltage drop which is then monitored and analyzed to determine the proximity sensing state. The costs of the proposed proximity sensor reduce to the fluorescent fiber and the electronics involved in the implementation of the proximity sensing logic. Extensive measurements validate the proposed solution for the distributed proximity sensor.

This article is organized as follows. The fluorescent fiber is modeled in Section 2, which provides a thorough description of fluorescence generation and propagation, as well as the spectral behavior. His information is then employed to design fiber measurement scenarios in Section 3 to characterize the fiber operation, followed by the description of the proposed proximity sensor in Section 4. Some conclusions are finally drawn.

2. The fluorescent fiber model

In this work, we have employed the red fluorescent fiber, code 81 0087 from Industrial Fiber Optics [2]. This fluorescent fiber operates on the principle of active optical fibers, widely employed in lasers and optical amplifier constructions. A fluorescent dye, used as a doping material, is distributed uniformly within the fiber core [21]. Down-conversion fluorescence is used for sensor construction. A light source, which emits with wavelength λ_1 within the visible spectrum, produces side illumination of the fiber and induces fluorescence with wavelength λ_2 in the visible spectrum. Wavelengths λ_1 and λ_2 are called the excitation and emission wavelength respectively, and follow

$$\lambda_1 < \lambda_2 \qquad (1)$$

as illustrated in the measured absorption and emission spectra of the red fluorescent fiber, depicted in Fig. 1 [11,22].

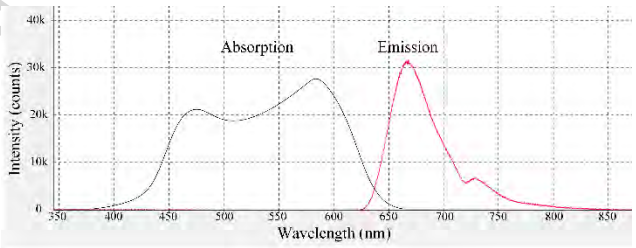

Fig. 1 Measured absorption and emission spectra of the red fluorescent fiber

Accordingly, light is generated within the fiber as a result of an incident light source. Operation of the fluorescent fibers is illustrated in Fig. 2 and is explained as follows.

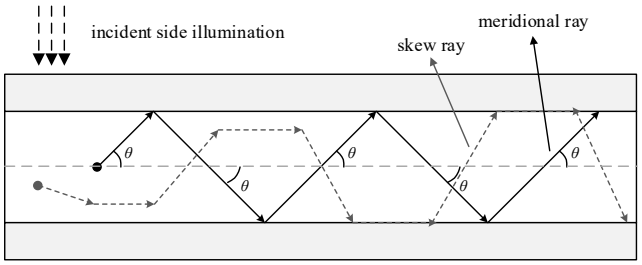

Fig. 2 Side view of the fluorescent optical fiber illustrating radiation generation as a result of incident side illumination

As illustrated, fluorescent radiation is the superposition of two types of rays, i.e. meridional and skew rays respectively, which are discussed as follows. The total fluorescence power per unit thickness can be expressed as

$$P_T = 4\pi \cdot \pi a^2 \cdot \rho \cdot pI \quad (2)$$

where a is the fiber core radius, ρ is the volume density of the fluorescent material, I is the source intensity and p accounts for the fluorescent emission probability per unit solid angle [21].

Meridional rays, generated by fluorescent particles situated on the fiber axis are depicted with solid line in Fig. 2. Let θ be the emission angle of such a fluorescent particle situated on the fiber axis. The condition for total internal refection (TIR) is expressed as

$$\cos\theta \geq \frac{n_{cl}}{n_{co}} \quad (3)$$

where n_{cl} and n_{co} are the cladding and core refractive indices respectively. The critical value θ_0 of the emission angle for TIR is then

$$\cos\theta_0 = \frac{n_{cl}}{n_{co}} \quad (4)$$

which gives the fraction of the total emission power generated by axial fluorescence expressed as

$$P_f = 1 - \cos\theta_0 \quad (5)$$

To be noticed is that, as resulting from (5), meridional rays only represent a small fraction of the total emission power. Skew rays on the other hand, coming from off-axis fluorescent particles and depicted with dashed line in Fig. 2, represent the consistent fraction of the fluorescent radiation and are the result of the uniform distribution of the fluorescent material within the fiber core [21]. The 3-dimensional illustration of skew rays, as depicted in Fig. 3, shows the azimuth φ and the elevation ($\pi/2 - \theta$) of the skew ray respectively, as well as the incidence angle β. Expression of the TIR condition for skew rays is then written

$$\cos\beta = \sin\theta \sqrt{1 - \left(\frac{r \cdot \sin\varphi}{a}\right)^2} \quad (6)$$

where r is the distance between the fiber axis and the fluorescent particle [21].

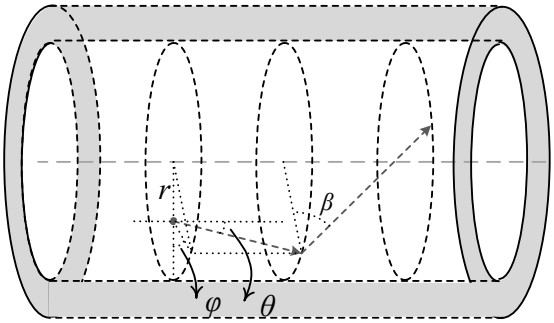

Fig. 3 3-dimensional view of the fluorescent optical fiber illustrating a skew ray

Then, the emission power contribution for narrow emission angles $\theta \subset [0, \theta_0]$ is written as [21]

$$P_N = P_T \cdot (1 - \cos\theta_0) \quad (7)$$

and the emission power contribution for wide emission angles $\theta \subset [\theta_0, \pi/2]$ is written as [21]

$$P_W = P_T \cdot (1 - \cos\theta_0) \cdot \cos\theta_0 \quad (8)$$

Equations (2), (7) and (8) enable the expression of the fluorescent fiber trapping efficiency [21]

$$TE = \frac{P_N + P_W}{P_T} = \frac{P_N + P_W}{4\pi^2 \cdot a^2 \cdot \rho \cdot p \cdot I} = 1 - \left(\frac{n_{cl}}{n_{co}}\right)^2 \quad (9)$$

Transmission of the fluorescence along the fiber follows an exponential attenuation expressed by Lambert-Beer's law

$$I_t = \eta \cdot I \cdot e^{-\alpha(\lambda)x} \quad (10)$$

where I_t is the transmitted light, η is a proportional measure of the total fiber illumination energy, x is the distance between the side illumination incidence point and the fiber end and $\alpha(\lambda)$ is the fiber attenuation coefficient [5, 7, 11]. The latter is further expressed as

$$\alpha(\lambda) = \rho \cdot \mu(\lambda) \quad (11)$$

where μ is the dye absorption coefficient. To be noticed is that equation (11) expresses the dependency of the fiber attenuation on the wavelength of the transmitted light through parameter μ which varies vs. the wavelength of the incident light [5, 11].

Finally, the fiber attenuation coefficient is used to define the fiber gain as

$$A_I = \frac{I_t}{I} = \eta \cdot e^{-\alpha(\lambda)x} \tag{12}$$

which is always below one, i.e. the fiber produces attenuation, since the intensity of the radiated fluorescence is smaller than the intensity of the incident light. Again, the fiber gain resembles a dependency on the wavelength.

The fiber emission spectrum is further on well described by the Moyal function plus a flat background [23, 24], expressed in expression (13):

$$f(\lambda,\mu,\sigma,A,B) = A \cdot \exp\left(-\frac{1}{2}\left(e^{-\frac{\lambda-\mu}{\sigma}} + \frac{\lambda-\mu}{\sigma}\right)\right) + B \tag{13}$$

where λ in the wavelength of the emission peak, A is the corresponding amplitude, σ is the spectral bandwidth, μ is the spectral shift of the emission peak due to the energy transfer mechanism [25, 26] and B is the flat, i.e. 0 order, background term.

The results of the measured spectra fits to Moyal functions, for the spectral measurements at LED distances ranging from 8cm to 20cm for this fiber type.

3. Operation of the red fluorescent fiber

Fluorescent optical fibers exhibit a variety of interesting applications reported in literature. Accordingly, it is important to understand and characterize the behavior of such fibers. In this work we analyzed a 81 0087 1mm red fluorescent fiber purchased from Industrial Fiberoptics [2]. According to the producer, the technical parameters of the fiber account for a 797 – 857 μm core diameter, 970 – 1030 cladding diameter, a step refractive index profile with a 1.6 core refractive index, and a 0.58 numerical aperture. A 1.5m long fiber was used throughput the experiments. The fluorescent fiber employed in this work exhibits a measured emission around 667nm. Measurements were carried out under ambient lighting conditions, and the fluorescent fiber exhibits a nominal emission power of P=6.2 μW.

Four measurement scenarios, which assume monitoring of the fiber emission power and photodiode voltage drop when the fiber end is applied to a photodiode, are listed in Table I and are presented as follows.

Table I Red fluorescent fiber measurement scenarios

Monitored fiber performance parameter	Illumination parameter
Fiber emission power vs.	Distance
	Height
Photodiode voltage drop vs.	Distance
	Height

The first measurement scenario assumed the measurement of the fiber emission power as a result of side illumination using a photometer. The test setup for this test scenario is illustrated in Fig. 4.

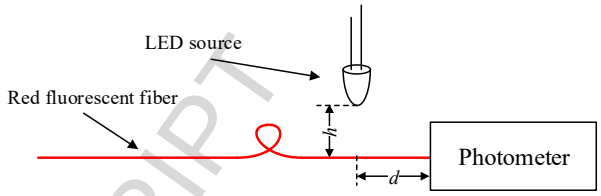

Fig. 4 Test setup for the determination of the fiber emission power vs. side illumination parameters

Four LED sources from a KMAC Educational Kit were used to perform side illumination of the fluorescent fiber: a blue LED (measured 462nm spectral peak), a green LED (measured 522nm spectral peak), a red LED (measured 660nm spectral peak), a white LED (measured broadband spectrum with 457nm blue spectral peak). The fifth light source was a CLM1C-WKW cool white high brightness LED (HBL) (measured broadband spectrum with 445nm and 567nm spectral peaks). The five light sources were successively used to apply side illumination to the optical fiber under the same measurement conditions: distance d = 10cm in-between the fiber illumination point and the powermeter, and a height h = 5cm of the LED referred to the fluorescent fiber. The measured LED emission power along with the corresponding fiber emission power are listed in Table II.

Table II Fiber emission power for various light sources

LED source	LED emission power	Fiber emission power	Normalized fiber emission
Red	5 μW	5.9 μW	1.18
Blue	10.2 μW	21.9 μW	2.15
Green	4.5 μW	10.6 μW	2.36
White	8.03 μW	19.8 μW	2.47
HBL	174 μW	75 μW	0.43

It is clear that the red fluorescent optical fiber exhibits the largest emission power for the HBL. This is motivated by the large HBL emission power, as well as by the overlapping between the broadband HBL emission and the fiber absorption spectra. To be noticed however is that the HBL requires the largest supply power for fiber illumination, and

will therefore be used for fiber saturation via axial illumination, rather than data transmission.

With respect to the LED incident light sources, which require considerably lower supply power in comparison to the HBL, the fiber is most sensitive to the blue LED. The cause is twofold. On one hand, the blue LED exhibits the largest emission power, and on the other hand the blue LED emission spectrum overlaps the fiber absorption spectrum. The blue LED is therefore suitable for transmission of binary information along the fiber, as is the case in the current work where we target the binary transmission of the sensor proximity state. On the other hand, red incident light has the lowest influence on the fiber emission power.

For an objective comparison however, the fiber emission power was normalized vs. the incident illumination power, also listed in Table II. This figure of merit illustrates that the blue, green and white LEDs exhibit similar yields for generating fiber fluorescence. Thus, our choice for the blue LED is furthermore motivated by the additional LED emission power which contributes the extra µW of fiber emission power required in the proposed sensing application. The HBL on the other hand exhibits the smallest yield for the same purpose.

The next measurement scenario accounts for variation of the distance d in-between the fiber illumination point and the photometer, with constant height h = 10 cm. Variation of the fiber emission power vs. the distance d is plotted in Fig. 5.

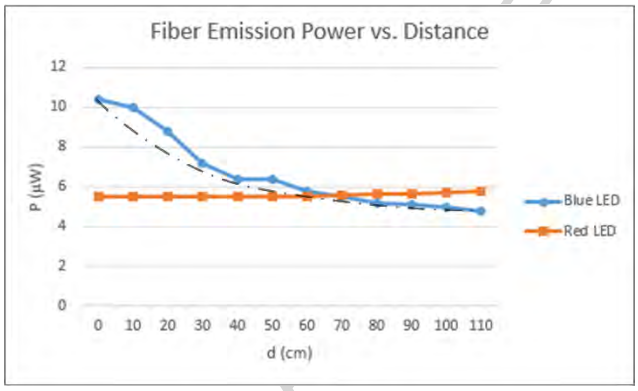

Fig. 5 Variation of the fiber emission power vs. distance

Under blue incident light, the fiber emission intensity exhibits an exponential decrease with the distance d, confirming equation (10). Indeed, the closer is the fiber illumination point to the fiber end, the larger will the fiber emission power be. Deviations from the exponential fitting curve, also plotted for reference in Fig. 5, are due to variations in the ambient fiber illumination caused by shadowing of the measurement setup. Red incident light on the other hand determines most insensitive behavior. This is due to the fact that the 660nm incident light from the red LED source is only slightly absorbed to produce fluorescent radiation, as illustrated by fiber absorption spectra in Fig. 1. In the same time, red light of shorter wavelength, e.g. 620-650 nm, would determine fluorescent radiation with rather low sensitivity vs. incident light. This is due to the rather large overlapping of the fiber absorption and emission spectra, as shown in Fig. 1 and as also specified in [11].

The next measurement scenario accounts for variation of the LED height h with respect to the fluorescent fiber. Only blue incident light is considered for this scenario. Variation of the fiber emission power vs. the height h is plotted in Fig. 6, illustrating a decrease of the fluorescent radiation power vs. the side illumination height.

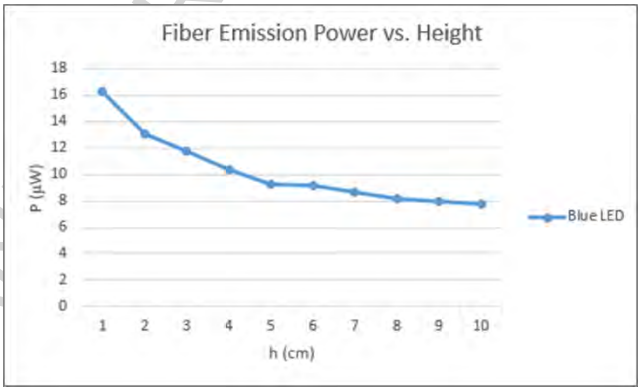

Fig. 6 Variation of the fiber emission power vs. height

The same behavior is observable when the fluorescent fiber is applied to a photodiode in the following test scenario, illustrated in the test setup from Fig. 7. The fluorescent fiber is applied to an Avago SFH250 photodiode. The reasons for choosing this photodiode were the “connector-less” package which allows the direct application of the optical fiber, integrated optical micro-lens for efficient optical coupling, as well as good sensitivity to red incident light [27].

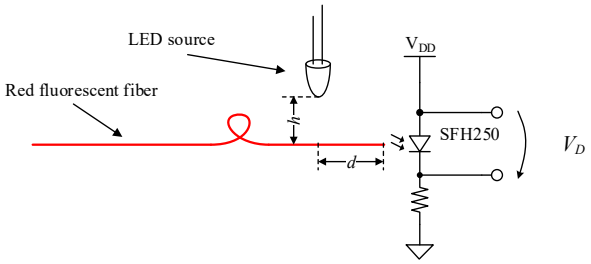

Fig. 7 Test setup for the determination of the photodiode voltage drop vs. side illumination parameters

In this setup, the diode voltage drop V_D was accounted to an estimate of the light intensity emitted by the fluorescent fiber under various illumination conditions. In laboratory environment, under ambient lighting with no additional fiber

illumination, the nominal diode voltage drop measures 240mV. Next, test scenarios account for varying the distance *d* in-between the photodiode and the fiber illumination point. Variation of the diode voltage drop vs. the distance *d* is plotted in Fig. 8, confirming the results formerly expressed in Fig. 5, namely that the red fluorescent fiber is indeed sensitive to side illumination with blue light following an exponential decrease with the distance *d*. The exponential fitting curve is also plotted for reference. Similarly to Fig. 5, Fig. 8 illustrates deviations of the photodiode voltage drop from the exponential characteristics, due to variations in the ambient fiber illumination and shadowing.

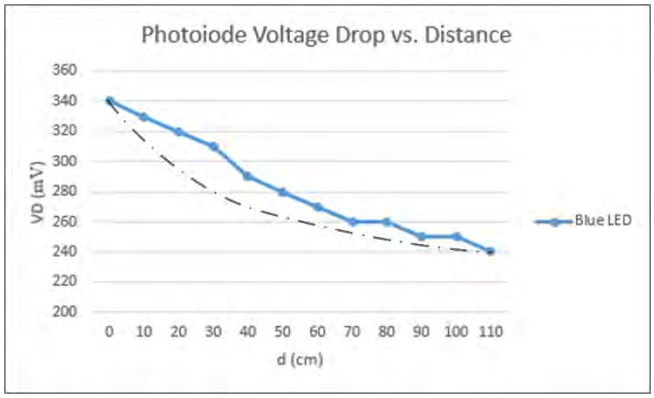

Fig. 8 Variation of the photodiode voltage drop vs. distance

The next measurement scenario accounts for variation of the blue LED height *h* with respect to the fluorescent fiber. Variation of the corresponding photodiode voltage drop vs. the height *h* is plotted in Fig. 9. Again, the results expressed from Fig. 6 are confirmed.

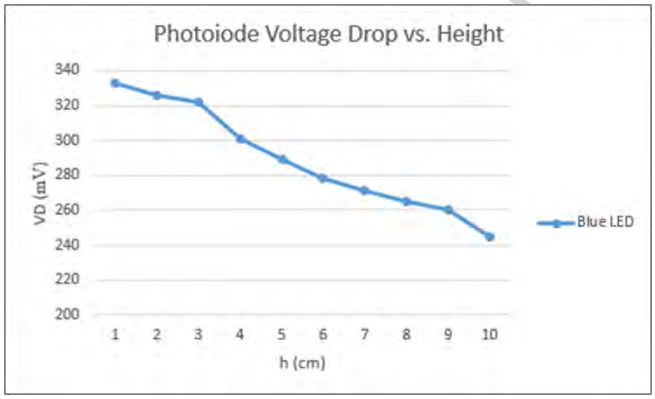

Fig. 9 Variation of the photodiode voltage drop vs. height

4. The proximity sensor laboratory proof of principle

The block diagram of the proposed proximity sensor is illustrated in Fig. 10. Operation of the proximity sensor is explained as follows. Passive resistance R operates towards forward biasing the photodiode. Accordingly, if no light is emitted by the fiber, i.e. the photodiode is dark, then there is no photodiode current. If on the other hand the fiber emits some light, there will be a proportional current flow I_D through the photodiode. The photodiode current I_D is then fed to a programmable transimpedance amplifier for current-to-voltage conversion. Next, a proximity indicator LED will be turned ON or OFF as prescribed by some proximity logic.

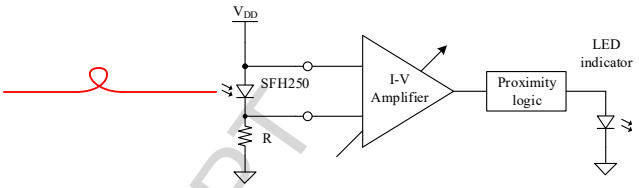

Fig. 10 Block diagram of the proposed proximity sensor

Operation of the proximity sensor imposes that emission of the fluorescent fiber is generated as a result of proximity sensing. This enables two operation scenarios. In the first scenario, illustrated in Fig. 11, an incident light source is attached to a moving object. When the moving object is sufficiently close to the optical fiber, i.e. the height of the incident light source is sufficiently small, the fiber emission intensity is large enough to turn ON the proximity indicator LED. This operation scenario accounts for direct proximity logic and is implemented with two inverters. The amplifier gain can be set large enough in order to have the amplifier output equivalent to a binary signal, encoding the "proximity" and "no proximity" states. The aim of the two inverters is for noise immunity, as they operate towards signal regeneration.

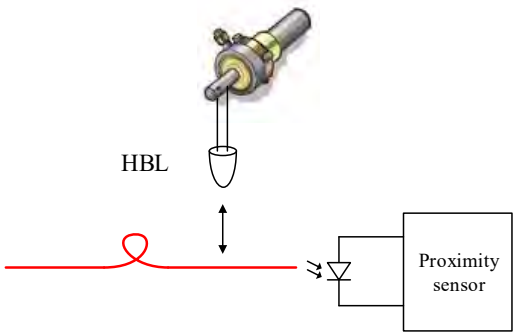

Fig. 11 Direct-logic proximity sensing scenario

To be noticed is that at least one of the two inverters should be Trigger Schmidt. Large fluctuations of the ambient illumination conditions may induce variation of the fiber emission intensity, accounting for noise in the electrical signal, as illustrated in Fig 12. This in turn determines parasitic switches of the amplifier output as the signal passes the switching threshold several times. This phenomenon is illustrated in time domain in Fig. 13 (a), followed by the corresponding voltage transfer characteristics (VTC) in Fig.

13 (b). Consequently, the logic circuit outputs erroneous proximity indication.

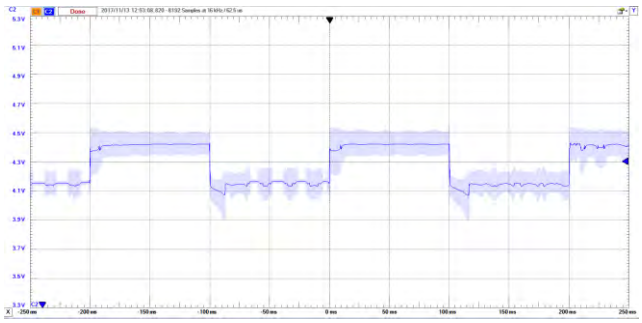

Fig. 12 Time-domain waveform of the photodiode voltage drop, in the presence of ambient light variations

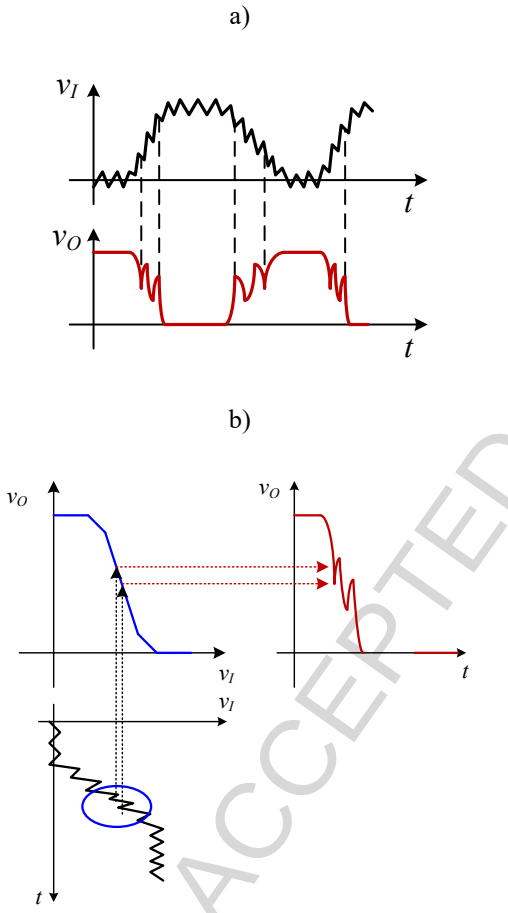

Fig. 13 a) Time-domain operation of the logic inverter and b) the corresponding VTC.

The Trigger Schmidt inverter imposes two different switching thresholds, V_{IH} for LOW→HIGH and V_{IL} for HIGH→LOW variations respectively, thus implementing a hysteresis inversion characteristics. Provided the hysteresis is wide enough, fluctuation of the fiber emission intensity won't generate parasitic switching of the LED driving signal. This phenomenon is illustrated in the time domain in Fig. 14 (a), followed by the corresponding voltage transfer characteristics (VTC) in Fig. 14 (b).

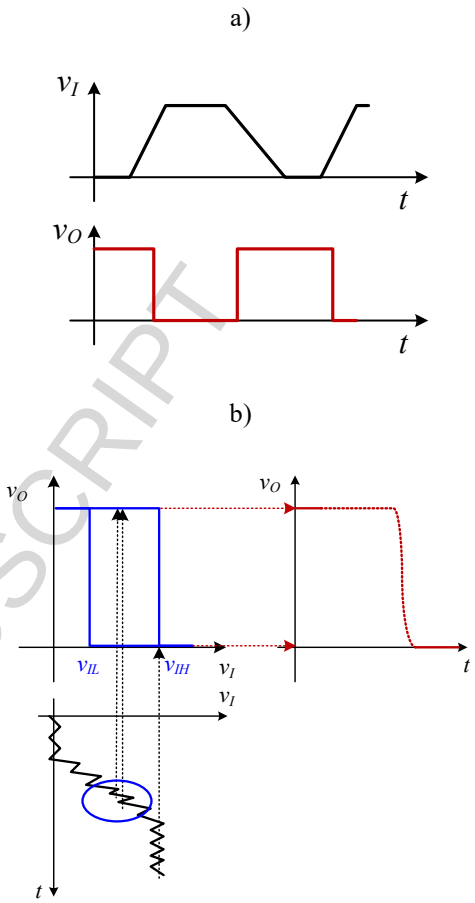

Fig. 14 a) Time-domain operation of the Trigger Schmidt inverter and b) the corresponding VTC.

The digital signal after the two inversions is illustrated in Fig. 15. Accordingly, after regeneration, the signal at the output of the Proximity sensing logic section is de-noised and won't affect the logic proximity state. Consequently, the sensor circuitry will only be sensitive to variations of the fiber emission intensity triggered by the fiber incident light source.

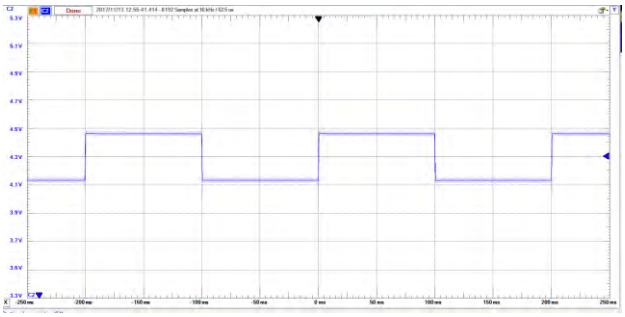

Fig. 15 Time-domain waveform of the digital signal at the output of the Proximity sensing logic section

Another issue which stands at this point is the intensity of the incident light source. As provided by the red fluorescent fiber characterization results, the HBL generates sufficient variation of the fiber emission intensity, and consequently sufficient variation of the photodetector current. The supply requirements for the HBL however impose a larger supply power in comparison to LEDs.

The second proximity sensing scenario, illustrated in Fig. 16, assumes the fiber continuously illuminated. In this case, the transimpedance amplifier output is always high. An obstacle, e.g. intruder, which comes between the incident light source and the fluorescent fiber will modify the fiber illumination conditions, thus reducing the fiber emission intensity. When the photodiode current becomes low enough, the amplifier output switches. This operation scenario accounts for complementary proximity logic and it is implemented with a single inverter. Motivation for using a Trigger Schmidt inverter is the same as before.

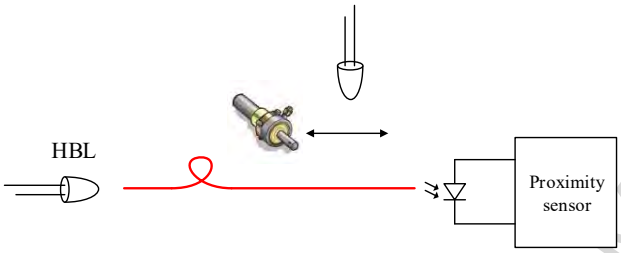

Fig. 16 Proximity sensing scenario following complementary logic proximity sensing

The issue with this proximity sensing scenario stands in the fiber illumination power. Neither a single HBL, nor a LED, deployed at a rather large height from the fiber won't generate sufficient incident power to keep the amplifier output high. Accordingly, the proposed solution employs fiber saturation via an axially deployed HBL at the other fiber end. The motivation for fiber saturation with HBL is that, in contrast to the other LEDs, the HBL delivers sufficient power into the fiber, and consequently generates sufficient illumination power, required for the proposed sensing application. Side illumination of the fiber for proximity sensing is then performed with the blue LED. The amplifier gain is set to have the output voltage equal to the switching threshold. Then, having an obstacle come in-between the blue LED and the fluorescent fiber will trigger the switching, thus turning the proximity state indicator ON.

A photograph of the laboratory test bench of the proposed proximity sensor is illustrated in Fig. 17. The proximity sensor was tested in both sensing scenarios: direct logic to sense the closeness of a moving object to the fluorescent fiber, and complementary logic to sense the interposition of a moving object in-between the incident light source and the fluorescent fiber. Laboratory measurements prove the correct operation of the developed proximity sensor.

a)

b)

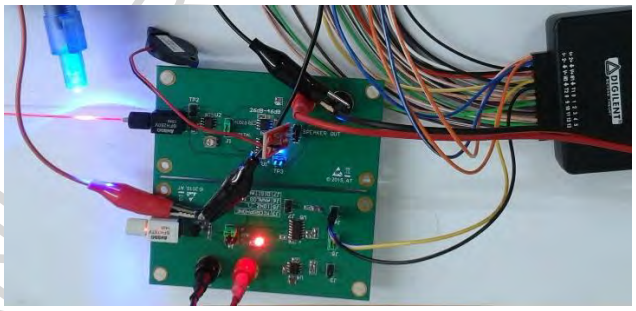

Fig. 17 Laboratory implementation of the proposed proximity sensor: a) printed circuit board and b) top view with acquisition board

5. Conclusions

This work presented a low-cost distributed proximity sensor implemented using a red fluorescent fiber. Operation of the proposed sensor relies on having the incident illumination intensity varied by the presence or absence of an obstacle in the vicinity of the sensing element. The fluorescence induced into the fiber by side illumination determines specific optical characteristics, useful in the proposed sensing applications. The employment of lateral excitation instead of axial excitation of the optical fiber allows for low-cost signal monitoring instrumentation to obtain accurate and robust measurements. The implementation of the proximity sensor was presented and experimentally verified. The obtained results validate the proposed concept, which can further be used for new applications of fluorescent polymeric optical fibers in optical sensor technology.

Acknowledgment

This work was financially supported by a grant of the Romanian National Authority for Scientific Research and Innovation, CNCS/CCCDI-UEFISCDI, project number PN-

III-P2-2.1-PED-2016-0172, within PNCDI III; also scientific supported from MPNS COST Action MP1401-Advanced fibre laser and coherent source as tools for society, manufacturing and lifescience.

References

[1] C. O. Egalon, Ocean Optics, Axial Versus Side Illumination of a Fluorescent Cladding Optical Fiber. Link - https://oceanoptics.com/wp-content/uploads/Claudio-Egalon-Axial-VS-Side-Illumination-of-a-Fluorescent-Cladding-Optical-Fiber.pdf, 01.11.2017.

[2] http://i-fiberoptics.com/fluorescent-fiber.php, 01.11.2017.

[3] Scintillating Optical Fibers, http://www.crystals.saint-gobain.com/sites/imdf.crystals.com/files/documents/sgc-scintillation-fiber_0.pdf, 01.11.2017

[4] C. O. Egalon, Multipoint side illuminated absorption based optical fiber sensor for relative humidity, Proceedings of SPIE - The International Society for Optical Engineering, 8847 (2013), doi: 10.1117/12.2024875.

[5] M. F. Laguesse, Optical potentiometer using fluorescent optical fiber for position measurement, Applied Optics, 28(23) (1989) 5144-8514.

[6] J. D. Weiss, A Fluorescent Long-Line Fiber-Optic Position Sensor, Sensors Online, (2005), http://www.sensorsmag.com/iot-wireless/a-fluorescent-long-line-fiber-optic-position-sensor, 29.08.2017.

[7] P. Aiestaran, V. Dominguez, J. Arrue, J. Zubia, A fluorescent linear optical fiber position sensor, Optical Materials, 31 (2009) 1101–1104.

[8] A. D. Bross, Scintillating plastic optical fiber radiation detectors in high-energy particle physics, Proceedings of SPIE, 1592 (1991) 122–132.

[9] R. A. Lieberman, L. L. Blyler, L. G. Cohen, A Distributed Fiber Optic Sensor Based on Cladding Fluorescence, Journal of Lightwave Technology, 8(2) (1990).

[10] C. Fitzpatrick, C. O'Donoghue, E. Lewis, A novel multi-point ultraviolet optical fibre sensor based on cladding luminescence, Meas. Sci. Technol, 14 (2003) 1477.

[11] M. F. Laguesse, M. J. Bourdinaud, Characterization of fluorescent plastic optical fibers for x-ray beam detection, Proceedings of SPIE – Plastic Optical Fibers, 1592 (1991) doi: 10.1117/12.50997.

[12] C. O. Egalon, Optical Fiber Chloride Sensor for Concrete Structures, Project Number 0109504, SBIR Phase I grant, National Science Foundation, 07/2001 to 12/2001.

[13] B. J. Prince, A. W. Schwabacher, P. Geissinger, A Readout Scheme Providing High Spatial Resolution for Distributed Fluorescent Sensors on Optical Fibers, Anal. Chem., 73 (2001) 1007-1015.

[14] J. L. Wu, Y. T. Wang, A Fluorescence Optic-Fiber Temperature Sensor Using Phase-Locked Detection with Pulse Modulation Single Reference, Journal of Physics: Conference Series, 48 (2006) 101–105.

[15] P. Miluski, M. Kochanowicz, J. Żmojda, D. Dorosz, "UV radiation detection using optical sensor based on Eu3+ doped PMMA" Metrology and Measurement Systems, 2016, 23 (4) (2016), 615–621, doi: https://doi.org/10.1515/mms-2016-0049.

[16] P. Miluski; D. Dorosz; M. Kochanowicz; J. Zmojda; J. Dorosz, Luminescent optical fibre sensor for UV-A detection, Proc. SPIE 9290, 2014, 92900G; doi: 10.1117/12.2075077

[17] P. Miluski, D. Dorosz, J. Żmojda, M. Kochanowicz, J. Dorosz, Luminescent polymer optical fibre sensor for temperature measurement, Acta Physica Polonica A, vol. 127 (2015).

[18] P. Miluski, D. Dorosz, M. Kochanowicz, J. Żmojda, Fluorescent polymeric optical fibre illuminator, Electronics Letters, 52(18) (2016), 1550 – 1552, doi: 10.1049/el.2016.1491.

[19] N. Cennamo, F. Mattiello, R. V. Galatus, E. Voiculescu, L. Zeni, Investigation of plasmonic sensing in D-shaped POFs with Fluorescent optical fibers used as light sources, IEEE Transactions on Instrumentation and Measurement, (2017) (accepted, publication in progress).

[20] R. Galatus, B. Feier, C. Cristea, N. Cennamo, L. Zeni, SPR based hybrid electro-optic biosensor for β-lactam antibiotics determination in water, SPIE Optical Engineering + Applications, (2017) (accepted, publication in progress).

[21] J. D. Weiss, "Trapping efficiency of fluorescent optical fibers", Optical Engineering, vol. 54, no. 2, 2015, doi:10.1117/1.OE.54.2.027101.

[22] P. Miluski, M. Kochanowicz, J. Żmojda, D. Dorosz, "Emission properties and energy transfer in Perylene-Rhodamine 6 G co-doped polymeric fiber", Chinese Optics Letters, vol. 14, no. 12, 2016, pp. 121602, DOI: 10.3788/COL201614.121602.

[23] Z. Papandreou, B.D. Leverington, G.J. Lolos, Spectral response of scintillating fibers, In Nuclear Instruments and Methods in Physics Research Section A: Accelerators, Spectrometers, Detectors and Associated Equipment, Volume 596, Issue 3, 2008, Pages 338-346, ISSN 0168-9002,

[24] G. Drexlin, V. Eberhard, D. Hunkel, B. Zeitnitz, Spectral attenuation length of scintillating fibers, In Nuclear Instruments and Methods in Physics Research Section A: Accelerators, Spectrometers, Detectors and Associated Equipment, Volume 360, Issues 1–2, 1995, Pages 245-247, ISSN 0168-9002

[25] Y. Yang, G. Qian, D. Su, Z. Wang, M. Wang, Energy transfer mechanism between laser dyes doped in ORMOSILs, Chemical Physics Letters 402 (2005) 389–394

[26] M. Kailasnath, N. Kumar, V.P.N. Nampoori, C.P.G. Vallabhan, P. Radhakrishnan, Excitation wavelength dependence of energy transfer in dye mixture doped polymer optical fibre preforms, Journal of Photochemistry and Photobiology A: Chemistry 199 (2008) 236–241

[27] Avago SFH250 datasheet, http://web.mit.edu/6.101/www/reference/AV02_fiber_receiver.pdf, 01.11.2017.